Original research article

Institution of MECHANICAL ENGINEERS
Journal of SYSTEMS AND CONTROL ENGINEERING

Proc IMechE Part I:
J Systems and Control Engineering
1–18

DOI: 10.1177/09596518261435665
journals.sagepub.com/home/pii
Sage

Comparative performance evaluation of meta-heuristic optimization algorithms for tuning PID gains in dual-axis solar tracking systems

Mohamed Ibrahem Taha[1], Mohamed A. Kamel[2], Ehab Said[2] and Wael Elmayyah[3]

Abstract

This work addresses the growing need for energy-efficient and accurate control in solar tracking systems, where precise alignment with the sun must be achieved without excessive actuator energy consumption. To this end, a novel proportional-integral-derivative (PID) controller tuning framework is proposed based on a dual-objective cost function that simultaneously minimizes both the integral time-weighted absolute error (ITAE) and the control effort, where the first objective is a measure of tracking accuracy, and the latter serves as a normalized approximation of control energy consumption. First, a complete model of the dual-axis solar tracking system is presented. Then, a PID controller is applied to minimize the tracking error. Next, the PID gains tuning is formulated as a multi-objective optimization problem, and five recent metaheuristic algorithms are applied to solve this problem. These algorithms are the Grey Wolf optimizer (GWO), the Aquila Optimizer (AO), the Manta Ray foraging optimization (MRFO), the Harris Hawks Optimization (HHO), and the gradient-based optimizer (GBO). All these algorithms are applied under consistent settings and benchmarked using 50 Monte Carlo simulations. Besides, they are compared based on their ability to achieve the best and mean solutions, standard deviation, computational effort, number of iterations, and convergence behavior. From the perspective of controller performance, the evaluation includes overshoot, settling time, steady-state error, and control energy consumption. Under these criteria, the GWO achieved the best cost values. All algorithms, however, exhibited overshoot limited to below 0.06% and settling times under 2 s. While from the perspective of algorithm performance, AO demonstrated the fastest average run-time and GWO was the lowest standard deviation, while MRFO achieved the lowest overshoot and GBO achieved the minimum energy consumption. The proposed framework outperforms existing approaches by integrating actuator energy into the control objective and validating statistical robustness through extensive simulation, thus offering a reliable, energy-aware strategy for real-time solar tracking deployment.

Keywords

Aquila Optimizer, dual-axis solar tracking systems, energy-aware control, gradient-based optimizer, Grey Wolf optimizer, Harris Hawks optimization, integral of time-weighted absolute error, manta ray foraging optimization, metaheuristic optimization, Monte Carlo simulation, proportional–integral–derivative control

Received: 8 September 2025; accepted: 24 February 2026

Introduction

The global shift to sustainable energy grids has immensely catalyzed the development and integration of solar photovoltaic (PV) technologies. Solar energy has become a pivotal pillar within decarbonization strategies due to its abundance, scalability, and rapidly plummeting costs. The utility-scale PV levelized cost of electricity (LCOE) has declined by over 80% over the last decade, making it one of the lowest cost sources of

[1]Department of Mechatronics Engineering, October University for Modern Science and Arts (MSA), Giza, Egypt
[2]Department of Mechatronics Engineering, Military Technical College, Cairo, Egypt
[3]Department of Mechanical and Aerospace Engineering, University of Strathclyde, Glasgow, UK

Corresponding author:
Mohamed A. Kamel, Military Technical College, Al-Khlaifa Al-Maamoon St, Cairo 11766, Egypt.
Email: mohamed.atef.kamel@mtc.edu.eg

energy.[1] The International Renewable Energy Agency (IRENA) states that global capacity of PV crossed 1 terawatt (TW) throughout 2024, and solar energy represented a significant proportion of newly installed renewable energy capacity.[2] These advances notwithstanding, its very variability engendered by the influence of diurnal cycle, clouds, and atmospheric states continues to impose constraints on energy yield, grid stability, and dispatchability.[3,4]

To tackle such issues and enhance energy harvesting efficiency, solar tracking systems have gained prominence. By actively moving PV panels to follow the trajectory of the sun, tracking systems reduce the loss caused by incident angles and attain optimal irradiance collection. To overcome these challenges and enhance energy harvesting efficiency, solar tracking systems have become increasingly important. By dynamically adjusting the orientation of photovoltaic (PV) panels to follow the sun's path, these systems reduce losses caused by non-optimal incidence angles and improve overall irradiance capture.[5]

Solar trackers are broadly classified into two main types: single-axis and dual-axis systems. Single-axis trackers rotate around a single axis—horizontal, vertical, tilted, or polar-aligned—to follow the sun's apparent motion during the day. They are mechanically simpler and more cost-effective than dual-axis trackers, require less power for operation, and are well-suited to large-scale utility installations.[5] However, their energy yield is lower than that of dual-axis systems, typically producing 10%–25% more energy than fixed-tilt arrays, and their efficiency decreases in high-latitude regions due to seasonal variations in the sun's path.[6] On the other hand, dual-axis solar tracking systems (DASTS) rotate along two perpendicular axes (azimuth and elevation) enabling precise sun alignment both daily and seasonally. These systems can capture maximum possible irradiance, delivering 20%–45% higher output than fixed-tilt configurations, and they perform especially well in installations where space is limited.[6,7] The trade-offs include greater mechanical and control complexity, higher initial investment and maintenance demands, and increased vulnerability to wind loads and mechanical wear.[8]

Because of their high energy yield and versatility, DASTS are widely adopted in precision-focused applications and in regions with significant seasonal shifts in solar position. Nonetheless, their advantages come with operational challenges, necessitating advanced control strategies to maintain high tracking accuracy, minimize energy use, and ensure long-term mechanical reliability. For comparisons among installed technologies, dual-axis solar tracking systems exhibit the largest performance increase, which on average increases energy production by 20%–45% compared to fixed-tilt installations.[1] These systems control both azimuth and elevation simultaneously, providing state-of-the-art tracking accuracy over seasons and geographical latitudes. However, installations using DASTS are subject to increased mechanical and control complexities, such as the need for precision tracking, highly synchronized actuator motion, and insensitivity to environmental disturbances like wind gusts and shading.[9]

In the literature, different control strategies have been applied to improve the performance of DASTS. High-performing control techniques are essential to ensure that DASTS operate efficiently and effectively under varying environmental and operational conditions. Several advanced approaches have been proposed such as fuzzy logic controllers (FLC),[10,11] adaptive neuro-fuzzy inference systems (ANFIS),[12] model predictive control (MPC), and sliding mode control (SMC). While these approaches exhibit improved nonlinear and uncertain control, real-time implementation is often constrained by computational and modeling constraints. On the contrary, proportional–integral–derivative (PID) controllers remain the industry standard due to their ease of implementation, economic feasibility, and functionality on low-power microcontrollers.[13,14]

Despite the widespread use of PID controllers, their performance in dual-axis solar tracking systems is often compromised by the system's nonlinearities, such as time-varying gravitational torque, friction, and wind load disturbances.[15] In practice, classical tuning rules like Ziegler–Nichols (Z-N) and Cohen-Coon remain popular due to their simplicity. However, these methods are derived under restrictive linear assumptions, valid only around a small operating point. They typically yield aggressive control actions characterized by high overshoot and excessive settling times when applied to nonlinear systems, leading to increased mechanical wear and energy waste. Furthermore, they lack the flexibility to explicitly handle physical constraints, such as actuator voltage saturation, which is critical in energy-limited solar tracking applications. To overcome these limitations, the tuning of PID gains has been increasingly formulated as a non-convex optimization problem. Unlike conventional gradient-based methods (e.g. gradient descent), which may lead to local optima for complex objective functions, metaheuristic algorithms offer a robust alternative. These population-based stochastic techniques are capable of exploring large, multimodal search spaces to identify global optima without requiring gradient information.[16]

In the context of solar tracking and renewable energy systems, evolutionary algorithms have established a strong track record. Early successful implementations utilized Genetic Algorithms (GA)[12] and Particle Swarm Optimization (PSO)[17] to minimize tracking errors. While effective, standard PSO and GA can suffer from slow convergence rates and sensitivity to initialization. Consequently, research has shifted toward more recent bio-inspired algorithms that offer improved exploration-exploitation capability. For instance, the Grey Wolf Optimizer (GWO) has been applied to optimize controller parameters for improved transient response.[18] Similarly, the Artificial Bee

Colony (ABC) algorithm has shown resilience in handling parameter variations.[15] Most recently, advanced metaheuristics such as the Aquila Optimizer (AO),[19] Whale Optimization Algorithm (WOA),[20] Harris Hawks Optimization (HHO),[21] and Manta Ray Foraging Optimization (MRFO)[22] have emerged, demonstrating superior convergence speed and precision in various engineering control problems.

Recent simulation-based optimization studies on DASTS have largely concentrated on minimizing tracking error metrics such as integral of squared error (ISE), integral of time-weighted absolute error (ITAE), or root mean squared error (RMSE), while overlooking control energy consumption and mechanical wear.[23] This narrow focus often leads to overactive control responses that achieve high trajectory accuracy at the cost of excessive actuator operation and elevated simulated energy demand.[24] Although some studies, such as the oppositional chimp optimization–PID,[25] incorporate low-energy criteria, such efforts remain uncommon. Another limitation lies in the absence of rigorous statistical validation in simulation-based research. Many studies assess only one or two algorithms and report single-run or best-run results without variance analysis, thereby neglecting performance variability and reproducibility.[26] Broader benchmarking efforts evaluating up to 20 algorithms for maximum power point tracking (MPPT)[27] and the multi-algorithm comparisons conducted[28] demonstrate that extensive comparative analysis is feasible, yet such approaches have rarely been applied to DASTS control. In this context, recent studies have also combined predictive control with adaptive metaheuristic optimization for MPPT, achieving fast convergence and reduced steady-state oscillations under rapidly changing irradiance and partial shading conditions.[29] Recent research has applied hybrid metaheuristic optimization techniques for tuning controller parameters in solar energy systems with battery storage, assessing control effectiveness via ITAE under varying irradiation, temperature, and load conditions in simulation environments.[30] Furthermore, the prevalent use of simple single-objective cost functions in simulation models fails to capture the trade-offs among tracking precision, energy efficiency, and actuator lifespan that influence real-world applicability. Multi-objective optimization strategies such as integrated parameter estimation with MPPT optimization[31] or Pareto-based multi-criteria designs[32] offer promise for balancing these competing objectives but remain underexplored in the solar tracking context.

To this end, and from the existing literature, the technical challenges regarding the control of DASTS can be summarized as follows:

1. High mechanical and control complexity: DASTS require precise synchronization of actuators, robust resistance to wind loads, and long-term mechanical reliability, which increases maintenance demands.[8,9]
2. Limitations of conventional controllers: While PID remains the industry standard due to simplicity and cost-effectiveness, it is highly sensitive to parameter tuning and struggles with nonlinear, time-varying system dynamics.[15]
3. Constraints of advanced control strategies: Although techniques like FLC, ANFIS, MPC, and SMC improve robustness in nonlinear and uncertain environments, their real-time applicability is limited by computational complexity and modeling requirements.[10,12]
4. Optimization shortcomings: Existing studies often rely on single-objective criteria (e.g. ISE, ITAE, RMSE) while neglecting control energy consumption, actuator wear, and multi-objective trade-offs such as efficiency versus lifespan.[23,24]
5. Limited benchmarking and validation: Many works compare only few algorithms, lack statistical robustness, and report single-run results without analyzing performance variability, which results in limited reproducibility.[20,26]

Motivated by the aforementioned issues, this research addresses the gaps by proposing an energy-aware, simulation-based, statistically robust, multi-objective optimization framework for DASTS control. First, the complete model of the DASTS is presented, where it is divided into four subsystems: the solar position algorithm (SPA), the solar irradiance subsystem, the electromechanical subsystem, and the PV subsystem. Then, PID control is applied to minimize the tracking error and also the control effort. To achieve these objectives, the PID tuning is formulated as a multi-objective optimization problem. Then, five metaheuristic optimization algorithms are presented to solve the optimization problem. These algorithms are: GWO, AO, MRFO, HHO, and the gradient-based optimizer (GBO). A fair comparative study among these five algorithms is illustrated under identical conditions. Moreover, the robustness of these algorithms is validated statistically based on Monte Carlo simulations and a non-parametric statistical analysis using Wilcoxon rank-sum test. Besides the comparative study between these five algorithms, the proposed tuning method is compared to recent state-of-the-art optimizations using PID control on solar trackers.

When comparing to the existing works, the main contributions of this research can be summarized as follows:

1. **Novel energy-aware tuning framework**: The PID tuning problem is formulated as a multi objective optimization problem that simultaneously minimizes ITAE and the cumulative control energy. To the best of the authors' knowledge, this specific energy-aware formulation for DASTS has not been presented or investigated in the existing literature;

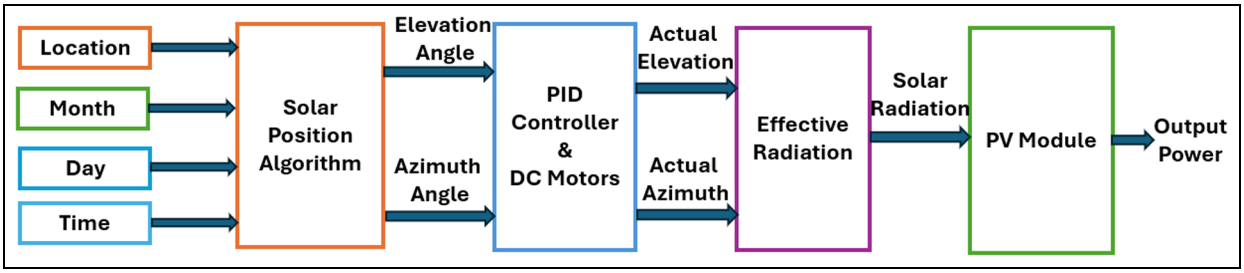

Figure 1. Block diagram of dual-axis solar tracking architecture.

2. **Comparative analysis of metaheuristic algorithms**: A comprehensive comparative study of five modern metaheuristic optimization techniques applied to this multi-objective problem is conducted. The analysis is performed under identical conditions, evaluating both the convergence characteristics of the optimizers and the dynamic performance of the controller; and
3. **Robust statistical validation**: The robustness of the proposed framework is validated through 50 independent Monte Carlo simulations for each algorithm, accompanied by non-parametric statistical tests using Wilcoxon rank-sum test to confirm the significance of the results.

The rest of this paper proceeds in the following manner: Section 2 offers the precise modeling of the DASTS including solar geometry, actuator dynamics, and system constraints. In Section 3, the development of the PID controller and the formulation of the PID tuning parameters optimization problem are highlighted. Section 4 introduces the five metaheuristic optimization methods and their application to the PID tuning optimization problem. In Section 5, extensive simulation analyses are presented. Finally, concluding remarks are highlighted in Section 6.

System modeling

The proposed DASTS consists of four interdependent subsystems: (1) the solar position algorithm (SPA); (2) the irradiance estimation on tilted surfaces; (3) the electromechanical drive system; and (4) the PV module model. These subsystems are not independent; rather, they interact to form a closed-loop system. The SPA provides the sun's position, which feeds into both the irradiance model and the control loop. The irradiance model determines the energy available on the tilted surface, the electromechanical model ensures that the tracker physically follows the calculated angles, and finally the PV model predicts the electrical power output. Together, these models form the foundation of a PID controller that is optimally tuned. The overall structure is illustrated in Figure 1.

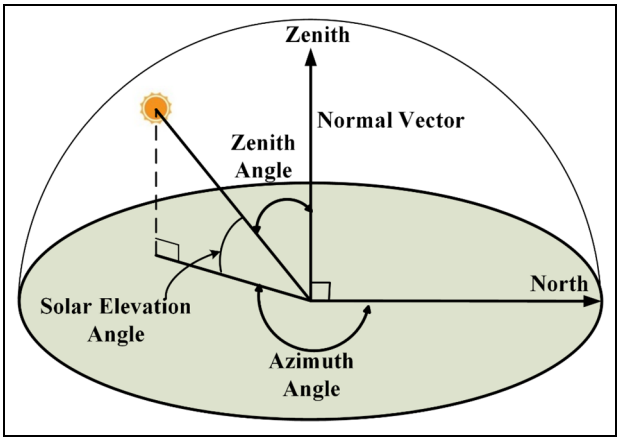

Figure 2. Solar angles.[33]

Solar Position Algorithm (SPA)

The SPA is the starting point of the DASTS model. It determines the sun's instantaneous position in the sky, expressed by two key geometric quantities: the *solar azimuth angle* (Az), which is the compass direction of the sun measured clockwise from true north, and the *solar elevation angle* (El), which is the angular height of the sun above the horizon, as illustrated in Figure 2. These two angles provide: (1) the reference orientation for the electromechanical tracker; and (2) the directional input required by the irradiance model to calculate the effective radiation on the PV modules. To obtain Az and El, the following steps are applied:

Step 1: Calculation of the day angle Γ_d: It accounts for the Earth's position in its orbit around the sun (in radians). It can be obtained as follows[34]:

$$\Gamma_d = \frac{2\pi}{365}\left(n_{\text{day}} - 1\right) \tag{1}$$

where n_{day} is the day of the year. Note that $n_{\text{day}} = 1$ for January 1st.

Step 2: Calculation of the *Equation of Time:* Because of Earth's elliptical orbit and axial tilt, the solar time differs slightly from the clock time. As a

result, a correction factor is needed. This correction factor is called the *Equation of Time* (EoT)[34]:

$$EoT = 229.18 \cdot (0.000075 + 0.001868\cos\Gamma_d - 0.032077\sin\Gamma_d - 0.014615\cos(2\Gamma_d) - 0.040849\sin(2\Gamma_d)) \quad (2)$$

where EoT is expressed in minutes.

Step 3: Calculation of the solar time ST: Based on the Equation of Time, the corrected solar time is then obtained as[34]:

$$ST = LT + \frac{4}{60}(L_{\text{std}} - L_{\text{loc}}) + \frac{EoT}{60} \quad (3)$$

where LT is local clock time (in hours), L_{std} is the standard meridian (in degrees), and L_{loc} is the local longitude (in degrees).

Step 4: Calculation of the hour angle H_a: It is defined as the sun's angular displacement east or west of the local meridian. From the solar time, H_a can be obtained as follows:

$$H_a = 15^\circ \cdot (ST - 12) \quad (4)$$

It can be noted that at solar noon, $H_a = 0^\circ$.

Step 5: Calculation of the declination angle δ_s: It specifies the latitude at which the sun is directly overhead at solar noon[34]:

$$\delta_s = 23.45^\circ \sin\left(\frac{360^\circ}{365}(n_{\text{day}} + 284)\right) \quad (5)$$

where δ_s oscillates between $\pm 23.45^\circ$ over the course of a year.

Step 6: Calculation of the solar elevation angle El: It is angular height of the sun above the horizon at a given location (ϕ_{loc}). It can be calculated as follows[34]:

$$El = \sin^{-1}(\sin\phi_{\text{loc}} \cdot \sin\delta_s + \cos\phi_{\text{loc}} \cdot \cos\delta_s \cdot \cos H_a) \quad (6)$$

This means that when $El = 0^\circ$, the sun is exactly at the horizon, and when $El = 90^\circ$, the sun is directly overhead (zenith).

Step 7: Calculation of the solar azimuth angle Az: It specifies the compass bearing of the sun, and can be obtained as follows[34]:

$$\sin Az = \frac{-\cos\delta_s \cdot \sin H_a}{\cos\theta_z} \quad (7)$$

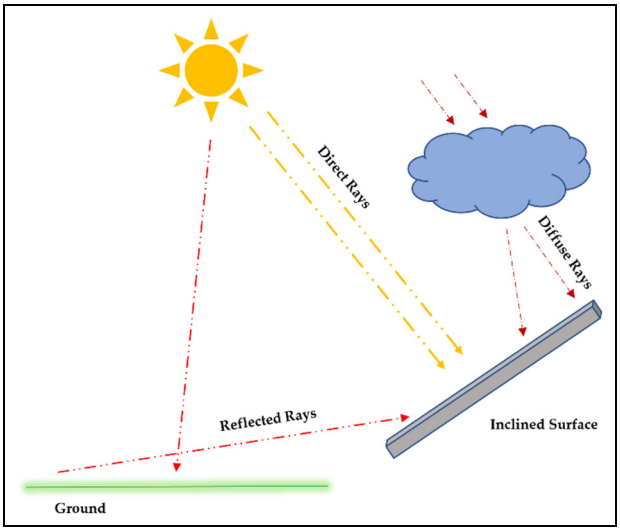

Figure 3. Types of solar irradiance on tilted surface.[37]

where θ_z is the zenith angle, and can be calculated as follows[34]:

$$\cos\theta_z = \sin\phi_{\text{loc}} \cdot \sin\delta_s + \cos\phi_{\text{loc}} \cdot \cos\delta_s \cdot \cos H_a \quad (8)$$

Here, $\theta_z = 90^\circ - El$. Thus, Az defines the horizontal direction of the sun, while El defines its vertical elevation.

To sum up, the SPA yields the pair (Az, El) which completely describes the apparent solar position in the sky. These angles are then used by: (1) the irradiance model to compute the solar radiation on the tilted PV surface; and (2) the control system as reference inputs for orienting the dual-axis tracker.

Solar irradiance on a tilted surface

With the solar position known, the next step is to determine the irradiance incident on the tilted PV modules. This is essential for both estimating the energy potential and providing input to the PV module model. Figure 3 illustrates the irradiance components. Using the Hay, Davies, Klucher, Reindl (HDKR) model,[35] the total irradiance G_T on the tilted surface [W/m^2] is[36]:

$$G_T = G_b R_b + G_d\left(\frac{1+\cos\beta}{2}\right)\left(1 + f\sin^3\left(\frac{\beta}{2}\right)\right) + G_h\rho_g\left(\frac{1-\cos\beta}{2}\right) \quad (9)$$

where G_b is the beam irradiance [W/m^2], G_d is the diffuse irradiance [W/m^2], G_h is the global horizontal irradiance [W/m^2], ρ_g is the ground reflectance, β is the tilt

angle [°], and f is the anisotropy index. The anisotropy index can be obtained as:

$$f = \frac{G_b}{G_b + G_d} \tag{10}$$

The beam tilt factor R_b is defined as a geometric ratio that quantifies how much more (or less) beam radiation a tilted surface receives compared to a horizontal surface. It can be calculated as:

$$R_b = \frac{\cos\theta_i}{\cos\theta_z} \tag{11}$$

with the incidence angle θ_i and zenith angle θ_z given in [°]. For instance, the incidence angle is:

$$\cos\theta_i = \sin\delta_s \sin(\phi_{\text{loc}} - \beta) + \cos\delta_s \cos(\phi_{\text{loc}} - \beta)\cos H_a \tag{12}$$

It can be noted that the computed G_T [W/m^2] serves as a direct input to the PV module model for electrical power estimation.

Electromechanical system modeling

The irradiance model defines the potential energy harvest; however, this potential can only be realized if the solar tracker accurately follows the reference orientation generated by the SPA. This task is achieved by the electromechanical drive system, which actuates the PV modules to align with the desired azimuth and elevation angles. The actuation is provided by a DC motor mechanically coupled to the tracker structure. Assuming a constant magnetic field and linear magnetic characteristics, the electromagnetic torque $T_m(t)$ [N· m] produced by the DC motor is directly proportional to the armature current $i_a(t)$, given by

$$T_m(t) = K_T i_a(t) \tag{13}$$

where K_T [N· m/A] is the motor torque constant. The back electromotive force (EMF) $E_b(t)$ [V], induced by the motor rotation, is proportional to the angular velocity $\omega_m(t)$ as

$$E_b(t) = K_E \omega_m(t) \tag{14}$$

where K_E [V· s/rad] is the back-EMF constant. Assuming that $K_E = K_T = K$, the coupled electrical and mechanical dynamics of the DC motor are described by

$$J_m \frac{d\omega_m(t)}{dt} + B_m \omega_m(t) + T_l(\theta(t)) = K i_a(t) \tag{15}$$

$$L_a \frac{di_a(t)}{dt} + R_a i_a(t) = v_a(t) - K\omega_m(t) \tag{16}$$

where J_m [kg· m^2] is the rotor moment of inertia, B_m [N· m· s/rad] is the viscous damping coefficient, L_a [H] is the armature inductance, R_a [Ω] is the armature resistance, and $v_a(t)$ [V] is the applied armature voltage.

In solar tracking applications, the DC motor drives a PV panel whose center of mass does not coincide with the axis of rotation. As a result, a gravitational load torque acts on the motor shaft, which varies nonlinearly with the angular position. This torque is modeled as

$$T_l(\theta) = mgl\sin(\theta) \tag{17}$$

where $\theta(t)$ is the angular position of the tracker, m is the equivalent mass of the PV module and supporting structure, g is the gravitational acceleration, and l is the distance between the rotation axis and the center of mass.

For position control, the angular velocity of the motor is related to the tracker position by

$$\frac{d\theta(t)}{dt} = \omega_m(t) \tag{18}$$

Substituting this relation into equation (15), the complete nonlinear electromechanical model of the solar tracker drive system is obtained as:

$$J_m \ddot{\theta}(t) + B_m \dot{\theta}(t) + mgl\sin(\theta(t)) = K i_a(t) \tag{19}$$

$$L_a \dot{i}_a(t) + R_a i_a(t) = v_a(t) - K\dot{\theta}(t) \tag{20}$$

The nonlinear dynamics of the solar tracker are expressed in state space form, where the state vector is defined as:

$$\mathbf{x}(t) = \begin{bmatrix} x_1(t) \\ x_2(t) \\ x_3(t) \end{bmatrix} = \begin{bmatrix} \theta(t) \\ \omega_m(t) \\ i_a(t) \end{bmatrix} \tag{21}$$

Considering the armature voltage $v_a(t)$ as the control input, the PV angular position $\theta(t)$ as the output, the affine nonlinear state-space model of the electromechanical subsystem can be formulated in the standard form:

$$\dot{\mathbf{x}}(t) = A\mathbf{x}(t) + Bu(t) + \boldsymbol{\eta}(\mathbf{x}(t)) \tag{22}$$

where the specific system matrices are given by:

$$\begin{bmatrix} \dot{\theta}(t) \\ \dot{\omega}_m(t) \\ \dot{i}_a(t) \end{bmatrix} = \begin{bmatrix} 0 & 1 & 0 \\ 0 & -\frac{B_m}{J_m} & \frac{K}{J_m} \\ 0 & -\frac{K}{L_a} & -\frac{R_a}{L_a} \end{bmatrix} \begin{bmatrix} \theta(t) \\ \omega_m(t) \\ i_a(t) \end{bmatrix} + \begin{bmatrix} 0 \\ 0 \\ \frac{1}{L_a} \end{bmatrix} u(t) + \begin{bmatrix} 0 \\ -\frac{mgl}{J_m}\sin(\theta(t)) \\ 0 \end{bmatrix}$$

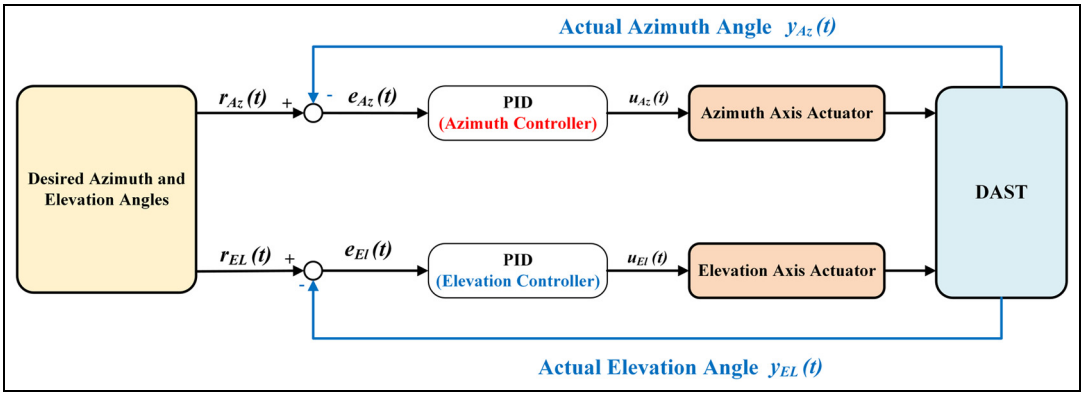

Figure 4. Control system block diagram of the DASTS.

$$y(t) = \begin{bmatrix} 1 & 0 & 0 \end{bmatrix} \begin{bmatrix} \theta(t) \\ \omega_m(t) \\ i_a(t) \end{bmatrix} \tag{23}$$

The presence of the nonlinear gravitational torque term $mgl\sin(\theta)$ introduces position-dependent dynamics into the system, which are particularly significant for elevation-axis tracking. This nonlinearity invalidates the use of a single linear transfer function over the full operating range. Therefore, controller design and performance evaluation are carried out using the nonlinear state-space model to ensure accurate and robust tracking of the SPA reference angle under varying gravitational loading conditions.

This electromechanical subsystem ensures that the physical tracker actuates the motors to the desired angles. The accuracy of this actuation directly influences the irradiance captured by the PV modules.

Photovoltaic module modeling

Once the tracker is properly oriented, the PV subsystem converts the captured irradiance into electrical power. This model links solar irradiance G_T and temperature T_c to the PV's electrical output (v_{pv}, i_{pv}), completing the energy conversion chain. In this way, the chain of models (from sun geometry to irradiance, electromechanical actuation, and PV conversion) forms an integrated description of the DASTS under closed-loop control. To derive the PV model, the total irradiance G_T from the HDKR model, combined with the cell temperature T_c [K], drives the single-diode PV model.[12] First, the terminal current of the PV module is calculated as follows[38]:

$$i_{pv} = i_{ph} - i_s\left[\exp\left(\frac{q\left(v_{pv} + i_{pv}R_s\right)}{n_{id}k_BT_c}\right) - 1\right] - \frac{v_{pv} + i_{pv}R_s}{R_{sh}} \tag{24}$$

where i_{pv} is the output current [A], v_{pv} is the terminal voltage [V], R_s and R_{sh} are the series and shunt resistances, respectively [Ω], q is the electron charge [C] (with $q = 1.602 \times 10^{-19}$ C), k_B is Boltzmann's constant [J/K] (with $k_B = 1.38 \times 10^{-23}$ J/K), n_{id} is the diode ideality factor, i_{ph} is the photo-current [A], and i_s is the diode saturation current [A]. The photo-current, dependent on irradiance and temperature, is:

$$i_{ph} = \left[I_{sc,ref} + K_I\left(T_c - T_{ref}\right)\right]\frac{G_T}{G_{ref}} \tag{25}$$

where $I_{sc,ref}$ is the reference short-circuit current [A], K_I is the temperature coefficient of current [A/K], T_{ref} is the reference temperature [K], G_T is the total irradiance on the tilted surface [W/m^2], and G_{ref} is the reference irradiance [W/m^2] (typically 1000 W/m^2). The diode saturation current varies with temperature as[38]:

$$i_s = I_{s,ref}\left(\frac{T_c}{T_{ref}}\right)^3 \exp\left[\frac{qE_g}{n_{id}k_B}\left(\frac{1}{T_{ref}} - \frac{1}{T_c}\right)\right] \tag{26}$$

where $I_{s,ref}$ is the reference diode saturation current [A], and E_g is the semiconductor band-gap energy [J].

Optimal PID controller design

This section presents the implementation of the optimal PID controller for the DASTS controller. The overall control system block diagram is shown in Figure 4. As mentioned before, DASTS must be constantly aligned with the sun to guarantee maximum energy harvesting throughout the day. To meet that objective, the controller must be highly precise, dynamically responsive, and robust against external perturbations such as wind or cloud cover.[39,40] Among the various available control methods, the PID controller is the most widely adopted due to its simplicity, computational speed, and proven track record in electromechanical systems.[15] However, the effectiveness of a PID controller relies heavily on proper tuning of its gain terms: proportional (K_p), integral (K_i), and derivative (K_d).

Traditional tuning methods such as Ziegler–Nichols often yield sub-optimal performance in nonlinear or multi-objective systems. To address these limitations,

the PID tuning is formulated as a constrained optimization problem, and is solved using metaheuristic algorithms that search for the near-optimal gain values. These optimized settings strike a balance between tracking performance and energy minimization.

Structure of PID

The continuous-time control law of the PID controller is given by:

$$u(t) = K_p e(t) + K_i \int_0^t e(\tau)d\tau + K_d \frac{de(t)}{dt} \tag{27}$$

Here, $u(t)$ is the control signal transmitted to the actuator, and $e(t) = r(t) - y(t)$ is the tracking error between the reference input $r(t)$ and the actual position $y(t)$. The response behavior of the controller is determined by the gain terms K_p, K_i, and K_d with the proportional term reacting to the present error, the integral correcting accumulated past error, and the derivative predicting future error trends.

For solar tracking applications, the controller must maintain accurate alignment with the sun while minimizing energy consumption. This is achieved using a multi-objective optimization approach that adjusts the PID gains accordingly.

Optimization problem formulation

To achieve the optimal PID controller performance for the DASTS, the optimal gains tuning problem can be declared as: finding the optimum gains K_p, K_i, and K_d that minimize both the tracking error and the energy consumption such that:

$$\min_u J(u), \tag{28}$$

$$J(u) = w_1 J_1(u) + w_2 J_2(u) \tag{29}$$

where $J(u)$ is the total objective function, $J_1(u)$ is the objective function that minimizes tracking error, $J_2(u)$ is the objective function that minimizes the energy consumption, w_1 and w_2 are weighting factors, and u is the vector of m design variables, such that

$$u = [K_p, K_i, K_d] \tag{30}$$

The values of J_1 and J_2 can be calculated as follows:

1. *Minimizing the tracking error:*

Different metrics are used to calculate the error like RMSE, integral of time-weighted squared error (ITSE), and ITAE. The RMSE takes into account the average of the squared deviations from desired trajectory and actual response and penalizes higher errors more. On the other hand, ITSE introduces a time-weighting factor to the squared error and penalizes late errors and thus encourages fast settling. Nevertheless, ITAE uses the absolute error and a time-weighting factor and penalizes not only steady-state error but also oscillations and encourages smooth behavior. Within these metrics, the ITAE is commonly used to fine-tune dynamic systems with minimal steady-state error and smooth transitions.[15,39] The ITAE can be calculated as follows:

$$J_1(u) = \int_0^T t|e(t)|dt \tag{31}$$

This term penalizes sustained tracking errors. The time-weighting factor t ensures that early transient errors are tolerated, but persistent errors incur increasing penalties. This enhances settling time and long-term accuracy, making the controller more responsive to trajectory deviations.

2. *Minimizing the control energy:*

In this work, the control energy is quantified as:

$$J_2 = \int_0^T u^2(t)dt \tag{32}$$

This term penalizes excessive control effort and provides a practical approximation of the electrical energy consumed by the DC motor during operation. The control signal $u(t)$ represents the voltage applied to the motor terminals. Under the assumption of a predominantly resistive load and negligible inductive dynamics, the instantaneous power drawn by the motor is proportional to the square of the applied voltage:

$$P(t) = c \cdot u^2(t) \tag{33}$$

where c is a constant dependent on the motor's electrical impedance. Therefore, the total electrical energy can be expressed as:

$$E = \int_0^T P(t)dt = \int_0^T c \cdot u^2(t)dt \tag{34}$$

This energy model follows the formulation in Maghfiroh et al.,[41] where $u^2(t)$ is used as a direct measure of control energy in comparative studies of DC motor controllers. Since the same motor is used across all test cases, the constant c is common and thus omitted for comparative analysis. This formulation is widely accepted in energy-aware control literature,[9,42] especially when detailed current measurements or dynamic impedance modeling are unavailable. Minimizing this term leads to smoother, more efficient actuation—reducing thermal load, enhancing motor longevity, and supporting sustainable operation in

resource-constrained or off-grid environments such as solar tracking systems.

The optimization problem is subjected to the following boundary constraints:

$$0.01 \leqslant K_p \leqslant 10 \tag{35}$$

$$0.01 \leqslant K_i \leqslant 10 \tag{36}$$

$$0.01 \leqslant K_d \leqslant 5 \tag{37}$$

$$-12 \leqslant u(t) \leqslant 12 \tag{38}$$

These bounds ensure that the resulting control actions are suitable for implementation on typical microcontroller-based platforms used in solar tracking systems. This dual-objective formulation facilitates the derivation of PID parameters that optimize both transient response and operational efficiency, key requirements for long-duration autonomous solar tracking applications.

Optimization algorithms

Effectively tuning PID controllers for complex, nonlinear, and time-varying systems such as DASTS presents a significant challenge due to the non-convex nature of the optimization problem. The effectiveness of a PID controller depends on achieving fast settling time, minimal overshoot, robustness to external disturbances, and reduced control energy consumption. Nevertheless, classical tuning techniques, including empirical approaches like Ziegler–Nichols or manual trial-and-error, often fall short when addressing real-world nonlinearities, environmental fluctuations, and stochastic dynamics. In light of these limitations, metaheuristic optimization algorithms have gained prominence in recent years as robust and versatile alternatives. These algorithms offer global search capabilities, require no gradient information, and perform well in high-dimensional, non-smooth, or multi-modal problems. Inspired by biological, ecological, or physical systems, meta-heuristics iteratively explore the solution space to identify the near-optimal solutions.

As mentioned earlier, five contemporary and widely cited metaheuristic algorithms are applied in this study to solve the multi-objective optimization problem of PID gains tuning. These algorithms are: GWO, AO, MRFO, HHO, and GBO. In this section, a brief overview of each algorithm is presented

Grey Wolf Optimizer (GWO)

The GWO is inspired by the leadership hierarchy and hunting mechanisms of grey wolves in nature.[43] Wolves are socially structured into four groups: α (leaders), β (advisors), δ (scouts), and ω (followers). Optimization is driven by the top three wolves guiding the rest of the pack. During the search, candidate solutions update their positions relative to the leaders, which ensures convergence toward the best regions of the search space. The balance between exploration (searching for new areas) and exploitation (refining current solutions) is naturally achieved by adjusting the influence of leaders over time. This structure enables GWO to efficiently converge to near-optimal solutions in nonlinear and high-dimensional problems.

Aquila Optimizer (AO)

The AO mimics the diverse hunting strategies of Aquila eagles, which include high soaring, targeted attacks, and perching.[44,45] The algorithm alternates between four main hunting modes depending on the search phase. In the early stages, global exploration dominates as the eagle soars and scans a wide area for prey. Later, the strategy switches to local exploitation, resembling rapid dives and precise attacks on identified targets. Random perturbations, such as Lévy flights, are integrated to help escape local optima. This multi-strategy design allows AO to adaptively transition between exploration and exploitation.

Manta Ray foraging optimization (MRFO)

MRFO is inspired by the cooperative feeding strategies of manta rays.[46] It simulates three primary behaviors: chain foraging, cyclone foraging, and somersault foraging. In chain foraging, rays follow one another in a sequence, enhancing collective movement toward food. Cyclone foraging involves a spiral movement that pushes the group closer to nutrient-rich regions, while somersault foraging allows sudden shifts toward the best-known positions. Together, these behaviors ensure diversity of solutions, strong local refinement, and robustness against premature convergence.

Harris Hawks Optimization (HHO)

HHO models the cooperative hunting style of Harris hawks, especially their surprise pounce strategy when targeting prey.[47,48] The algorithm uses the concept of prey escape energy to determine whether the hawks should explore globally or exploit locally. When the prey is "energetic," hawks spread out to explore; when the prey weakens, they encircle and launch coordinated attacks. The inclusion of random movements and surprise pounces enhances the balance between diversification and intensification, enabling HHO to efficiently solve a wide range of optimization problems.

Gradient-based Optimizer (GBO)

The GBO integrates gradient-inspired concepts with population-based metaheuristics.[49] Unlike purely nature-inspired methods, GBO leverages directional information to accelerate convergence. It forms a

Table 1. PV module specifications (120 W).

Parameter	Value	Parameter	Value
Power	120 W	V_{oc}	22.3 V
I_{sc}	6.8 A	V_{mp}	18.0 V
I_{mp}	6.7 A	R_s	0.45 Ω
R_{sh}	100 Ω	Diode factor n	1.3

guiding vector from the best-performing solutions and combines it with random interactions among agents to maintain exploration. This hybrid approach enables GBO to exploit promising regions more effectively while avoiding stagnation. Its strength lies in combining the efficiency of gradient-based learning with the global search capability of metaheuristics, making it particularly effective for high-dimensional and complex landscapes.

Results and discussion

The above-mentioned optimization problem is solved using five different meta-heuristics. Simulations were executed in MATLAB® to evaluate the performance of the proposed PID tuning approach under realistic operating conditions. All simulations were performed on a high-performance computing environment comprising an Intel Core i7-12700H processor, 16 GB of RAM, a 100 Hz sampling frequency, and a 64-bit Windows 11 Pro operating system.

The geographical setting of Giza, Egypt (Latitude: 30.0131° N, Longitude: 31.2089° E, GMT + 2) was selected as a high-sunlight region ideal for solar tracking studies. The test date was May 5th, 2025. The simulations were based on a clear-sky scenario using local solar position parameters and irradiance models. A commercial 120 W photovoltaic module was modeled using the single-diode equivalent circuit with irradiance and temperature-dependent current-voltage characteristics. The parameters of the PV module were selected to reflect realistic hardware values typically used in small- to medium-scale solar tracking setups. Table 1 summarizes the electrical characteristics used in the simulations.

A total of 50 Monte Carlo simulations were conducted per algorithm to ensure statistical significance. To ensure reproducibility of the meta-heuristic optimization results, a fixed random seed was applied across all Monte Carlo simulations. Specifically, MATLAB's global random stream was initialized using rng(1) prior to each algorithm run. This guarantees consistent pseudo-random behavior for population initialization and algorithmic stochastic operators, enabling fair comparison across the five meta-heuristics and repeatable benchmarking experiments. Each meta-heuristic ran with a population size of 50 and a maximum of 100 iterations. An early stopping criterion was employed to halt optimization if no change in the cost function within a range of 0.05 was detected over 10 consecutive iterations. The cost function was a weighted sum of J_1 and J_2. The main optimization hyperparameters, algorithmic strategies, and update rules for each method are described in Tables 2 and 3, respectively.

Table 2. Common hyperparameters and simulation settings used for all optimizers.

Item	Value
Population size	$N_{pop} = 50$
Maximum iterations	$T_{max} = 100$
Stopping criterion	Tolerance $\tau = 0.05$ for 10 consecutive iterations
Weighting factors	$w_1 = 0.8$, $w_2 = 0.2$
Simulation step	$\Delta t = 0.005$ s
Simulation horizon	$T = 5$ s
Reference input	Unit step $r(t) = 1$
Random seed	Fixed seed for reproducibility

Optimization results

Figure 5 illustrates the cost function convergence of all algorithms under the nonlinear torque load. It can be seen that all methods converge rapidly, typically within approximately 10–20 iterations, indicating efficient search and stable termination behavior. However, GWO, AO, MRFO, and HHO reach close objective levels with early stabilization, while GBO converges to comparatively higher cost values and exhibits slower improvement.

Figure 6 shows a boxplot comparison for overshoot, cost function, and control energy values derived from the 50 independent Monte Carlo simulations. It can be seen from Figure 6(a) that all algorithms maintain low overshoot levels, while GBO exhibits the highest overshoot tendency. Moreover, Figure 6(b) indicates that GWO attains the lowest and most compact cost spread, whereas AO, MRFO, and HHO remain competitive but with larger variability, and GBO yields higher costs overall. Besides, Figure 6(c) reports the control-energy distributions, demonstrating comparable effort levels across algorithms with small differences in the best-achieved energy values.

The average number of iterations and corresponding computational time per run is shown in Figure 7. It can be noticed that AO completes the optimization in the shortest time (1.241 s) using an average of 12 iterations. However, GWO exhibits the highest computational demand, requiring 1.504 s and 13.9 iterations on average. These results support the real-time applicability of AO for embedded solar tracking systems.

Statistical significance analysis

To statistically validate the comparative performance of the evaluated algorithms under the nonlinear torque load, non-parametric hypothesis testing was conducted

Table 3. Detailed meta-heuristic parameters and strategies used in PID tuning.

Algorithm	Step size/update rule	Control parameter(s)	Mutation/randomization strategy
GWO	Weighted average of α, β, δ wolves	$a \in [2 \rightarrow 0]$, r_1, r_2 uniformly random	Leadership hierarchy-based exploration; random coefficient updates per dimension
AO	Elite-based attraction and Lévy-driven steps	φ = rand(), λ = 1.5	Random global–local transition or differential agent vector update
MRFO	Directional drift using Lévy or Brownian motion	$s(t) \sim$ rand()	Elite-biased perturbation or directional difference of random peers
HHO	Prey escape modeled by energy reduction	$E_0 \in [-1, 1]$, $E = 2E_0(1 - t/T)$	Random jump strength with escape-energy-based switching behavior
GBO	Mean-vector guided motion with stochastic difference vectors	r_1, r_2 randomly drawn from $[0, 1]$	Directional update via agent-to-agent difference scaled by random weights

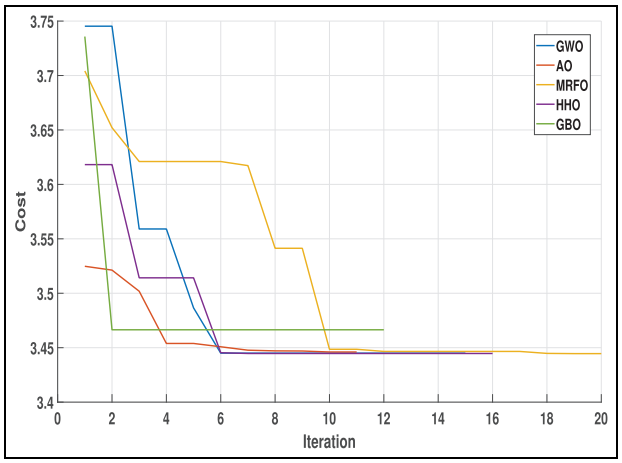

Figure 5. The objective function values history along the number of iterations.

based on the cost values obtained from 50 independent Monte Carlo runs. Preliminary assumption checks using the Lilliefors and Levene tests[50] revealed violations of normality and homogeneity of variances, respectively; therefore, parametric ANOVA was deemed inappropriate. Accordingly, pairwise comparisons were performed using the Wilcoxon rank-sum (Mann-Whitney U) test. Since multiple comparisons were required, Holm correction was applied to control the family-wise error rate. The numerical outcomes are reported in Table 4, while Figures 8 and 9 provide a compact visual summary of the adjusted and raw p-values, respectively.

As summarized in Table 4, AO, MRFO, and GBO exhibit statistically significant differences in cost compared to the GWO baseline at $\alpha = 0.05$, whereas HHO does not show a statistically significant difference relative to GWO. These statistical outcomes are consistent with the significance patterns illustrated in Figures 8 and 9.

Control system results and performance

Figure 10 presents the closed-loop step responses of each PID-tuned controller and the classic Ziegler-Nichols (Z-N) baseline. It is evident that the Z-N tuned PID exhibits significant overshoot and a prolonged settling time, which is characteristic of its tuning nature. In contrast, all metaheuristic-based controllers produce well-damped responses with overshoots below 0.2% and settling times between 1.82 and 1.93 s, demonstrating clear superiority over the Z-N method. Among the metaheuristics, AO achieves the fastest rise time and MRFO achieves the lowest overshoot.

Regarding the steady-state error, Figures 11 and 12 show both the elevation and azimuth tracking behavior, respectively under sudden trajectory changes. It can be noted that under all meta-heuristics, the PID controllers exhibit strong robustness, negligible steady-state error, and rapid re-convergence to the target trajectory. Also, Figure 13 shows the error trajectories $e(t)$. The Z-N controller shows a slower decay rate of the tracking error compared to the proposed approach. Under all metaheuristics, the PID controller exhibits rapid error decay, with AO providing the fastest convergence to zero error, which is consistent with its transient performance metrics.

From the point-of-view of control effort, Figures 14 and 15 display the control signal $u(t)$ and energy $u^2(t)$, respectively. The Z-N method produces high magnitude control actions, leading to higher energy consumption. Conversely, the metaheuristic algorithms generate smoother control signals with reduced energy variance. Specifically, GWO and GBO deliver slightly smoother control actions than the others, but all proposed algorithms significantly outperform the Z-N baseline in terms of energy efficiency.

To sum up, and after 50 executions of all meta-heuristics, Tables 5 and 6 summarize the optimal PID parameters, cost values, statistical standard deviations (STD), overshoot, settling time, average computation time, and control energy for each algorithm. It is observed that GWO and MRFO consistently achieve the lowest STD values, indicating reliable performance across Monte Carlo executions. In contrast, HHO shows the highest variability, reflecting less dependable convergence. Overall, the results demonstrate that the proposed energy-aware PID tuning methodology significantly enhances tracking accuracy and control

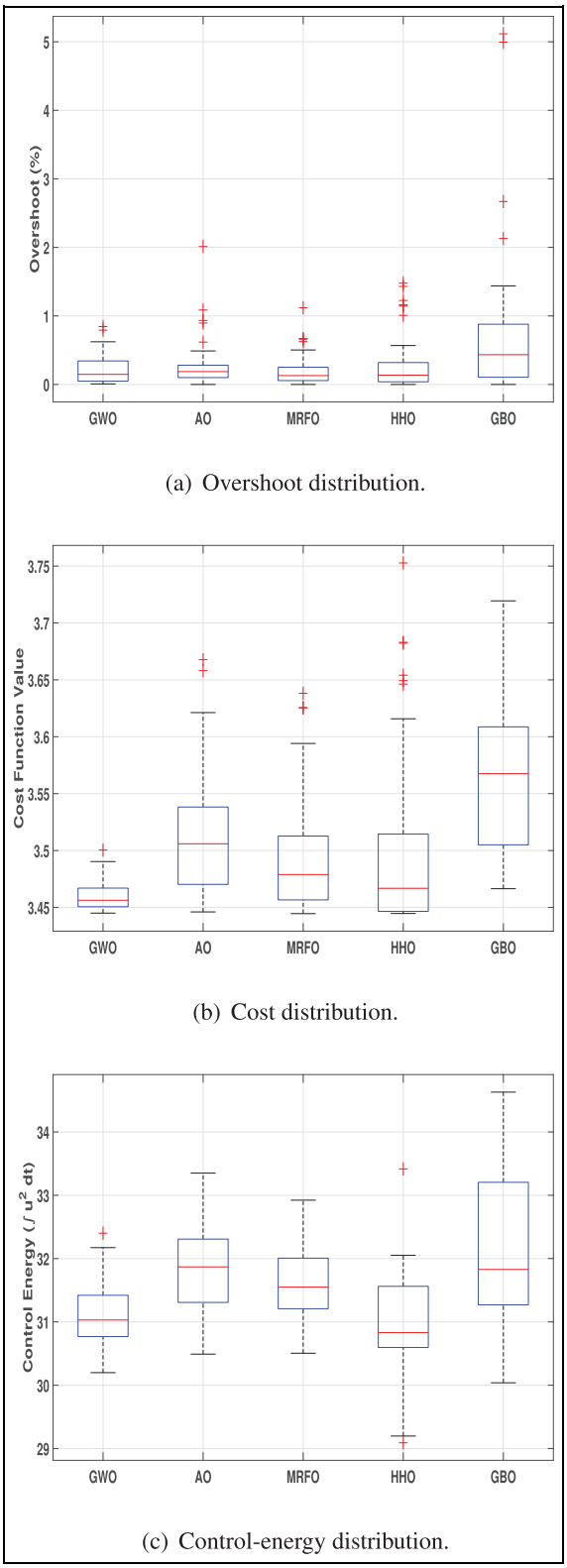

(a) Overshoot distribution.

(b) Cost distribution.

(c) Control-energy distribution.

Figure 6. Overshoot, cost function, and control energy distributions over 50 Monte Carlo runs for all five algorithms: (a) overshoot distribution, (b) cost distribution, and (c) control-energy distribution.

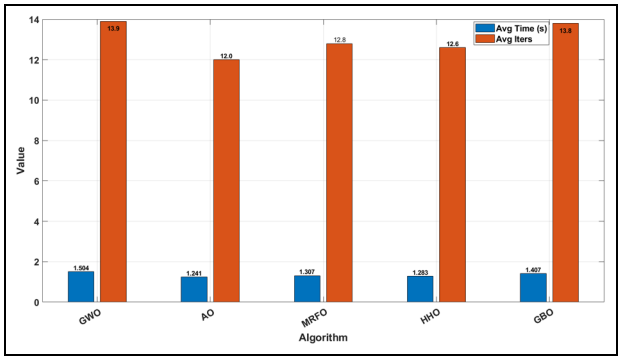

Figure 7. Average computational time and iterations for each algorithm.

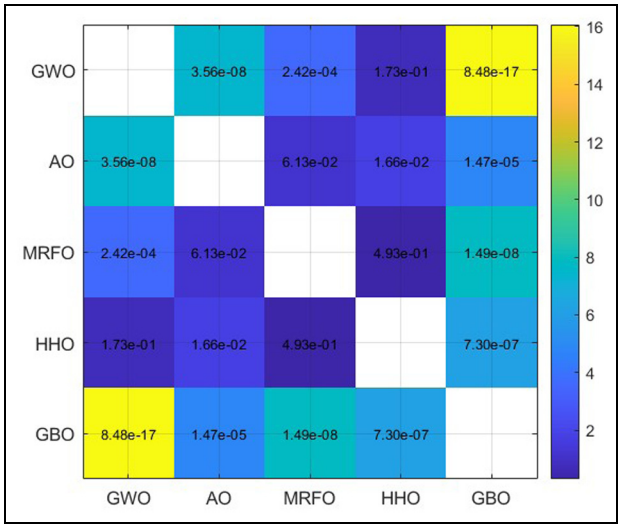

Figure 8. GWO-reference Wilcoxon rank-sum p-values with Holm correction for COST (50 runs). Color encodes $-\log_{10}(p)$.

Table 4. Wilcoxon rank-sum test on cost values versus GWO with Holm correction ($\alpha = 0.05$).

Comparison	Median cost	Holm-adj. p	Sig.
AO vs GWO	3.5059	1.07×10^{-7}	Yes
MRFO vs GWO	3.4789	4.83×10^{-4}	Yes
HHO vs GWO	3.4668	1.73×10^{-1}	No
GBO vs GWO	3.5675	3.39×10^{-16}	Yes

efficiency. Among the evaluated methods, GWO and AO stand out as the most suitable for real-time embedded solar tracking applications due to their convergence speed, stability, and actuator-friendly control profiles. As a result, power analysis of the DASTS under GWO-tuned PID controller will be investigated.

GWO-PID controller's output power analysis

Figure 16 illustrates the output power evolution as a function of time for the GWO-tuned PID-controlled over the daylight hours. The maximum rated PV module test-condition output power is indicated as a dashed

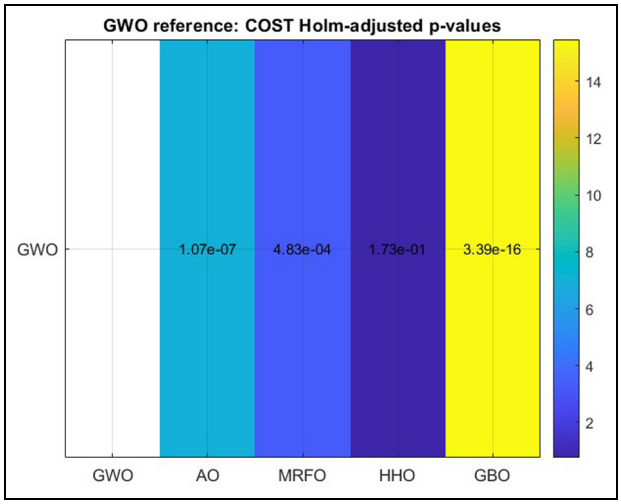

Figure 9. Pairwise Wilcoxon rank-sum raw p-values for COST (50 runs). Color encodes $-\log_{10}(p)$.

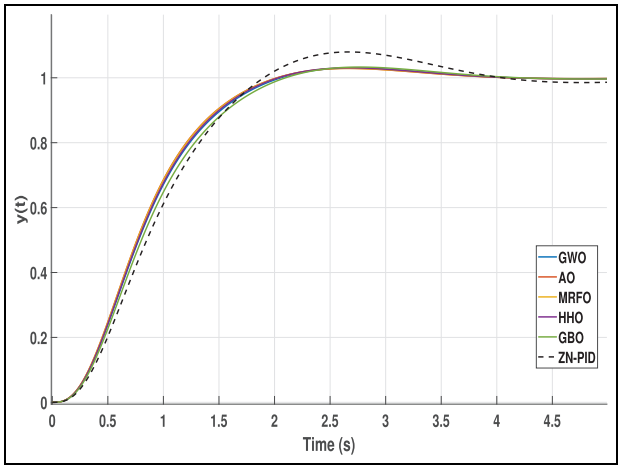

Figure 10. Step response analysis.

line at 120 W. The GWO-PID controller shows very good harvesting properties for the power, as shown from output levels almost reaching the reference value in the most illuminated hours (roughly between 11:00 and 13:00 h). The curve profile is smooth and bell-shaped symmetrically around noon, in line with the typical daily solar light regime on a clear day. Interestingly, the controller produces peak output near 121 W, so the system can operate at or just a little higher than nameplate capacity for the panel in full alignment to the sun. This is a testament to just how effective the GWO algorithm in ensuring the panels are positioned for maximum illumination. Besides, the absence of oscillations or sudden power changes in the power profile is an indication of good stability for the controller and good tracking precision. The smooth ascendance and descent in power at sunrise and sunset further confirm minimal overshoot or lag in the actuators, affirming the adequacy of the optimized PID

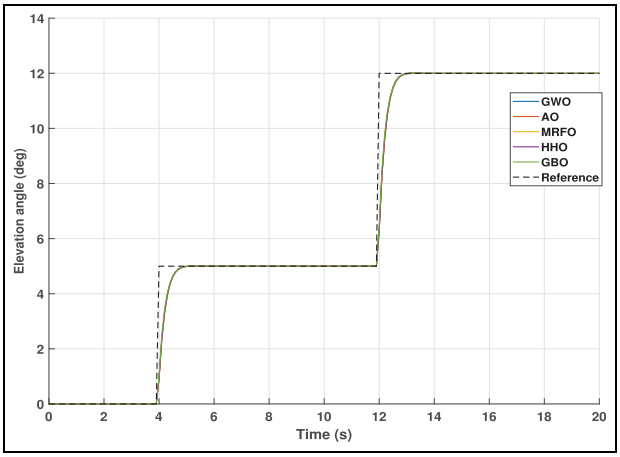

Figure 11. Elevation tracking performance during sudden trajectory changes.

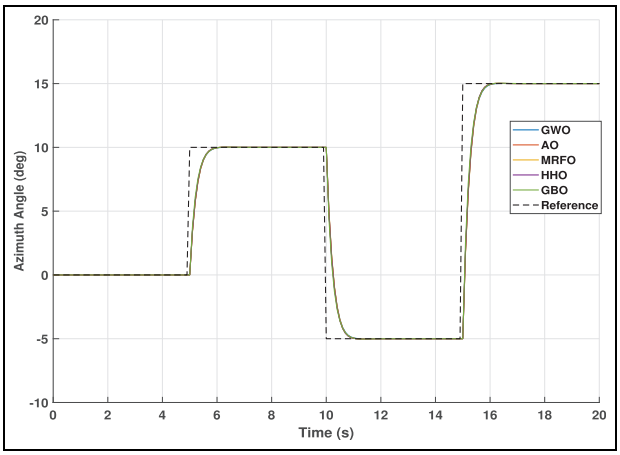

Figure 12. Azimuth tracking performance during sudden trajectory changes.

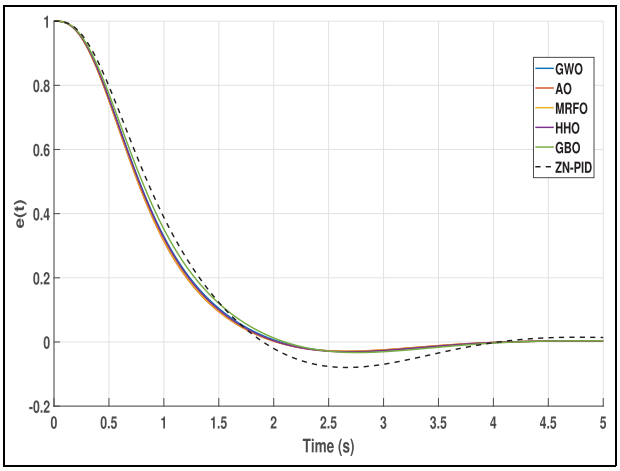

Figure 13. Tracking error $e(t)$ for all algorithms.

gains for the GWO. The energy performance metric, in the value of $\int u^2(t)dt = 30.5772\,\mathrm{V}^2$ s, is also among the

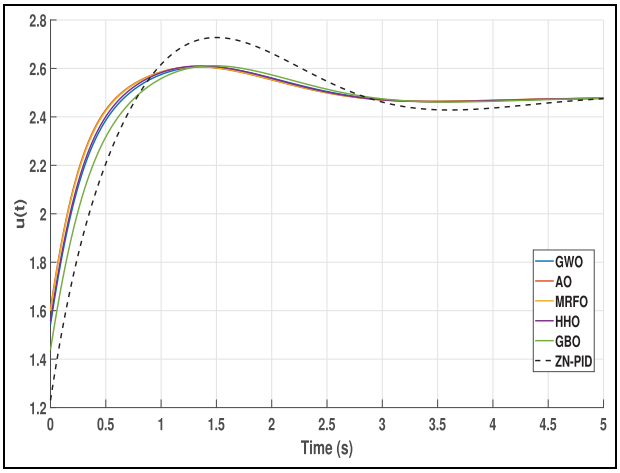

Figure 14. Comparison of control signal $u(t)$ for all algorithms.

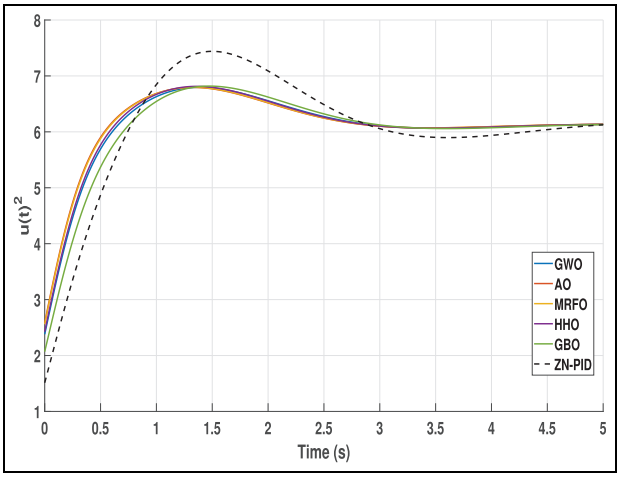

Figure 15. Squared control signal $u^2(t)$ that represent energy expenditure.

lowest for all algorithms tested, showcasing GWO-PID controller's capacity to ensure energy efficiency as well as good tracking precision.

In conclusion, the GWO-PID controller provides stable, real-time control for power with extremely minimal energy loss for transitional sun positions. This is consistent with the broader study results, where GWO produced the lowest overshoot (0.06%) and a similar settling time (1.87 s), which made it one of the best solar tracking control strategies in terms of energy efficiency.

Comparison with related works

To verify the proposed control algorithm, the performance of the GWO-PID controller is compared with that of various recent solar tracker tuning work available in the literature. Comparison is based on overshoot, settling time, and energy performance. Table 7 summarizes this comparison.

In Mazumdar et al.,[51] GWO was implemented without taking energy into account, thereby yielding a higher overshoot (0.25%) and larger settling time ($\approx$ 1.2 s) compared to the overshoot of 0.13% and settling time of 0.78 s obtained with the proposed AO-PID controller. Also, in Chauhan et al.,[52] artificial neural network (ANN)-PID hybrid controller was implemented achieving moderate transient performance (0.20% overshoot and 1.0 s settling), but lacking energy awareness or statistical robustness across multiple runs in contrast to the proposed algorithm in this work. Moreover, in Taha et al.,[11] PSO-PID consistently outperforms FLC, achieving negligible tracking errors (0.006°/0.002 °) and 0.19%, although their analysis was limited to one optimization method and did not consider control energy consumption. Likewise, in Rawat et al.,[53] the PID gains are tuning by means of GA, PSO, and teacher-learner-based optimization (TLBO). Results show that TLBO achieved the most robust results with only 0.012% overshoot and a rapid 0.0538 s settling time. However, their work primarily focused on robustness against parametric uncertainties without assessing energy efficiency in a dual-axis solar tracker. By contrast, the proposed AO-PID not only improves transient metrics (0.06% overshoot and 0.77 s settling time) but also minimizes control energy to 7.3997 V^2s, demonstrating a significant advancement over both conventional and earlier meta-heuristic-based approaches. Overall, the results clearly indicate that the developed dual-objective, meta-heuristic optimized PID controllers provide superior dynamic response and energy efficiency compared with existing techniques, with higher statistical rigor and reproducibility.

Remark 1. The results cited in Table 7 originate from diverse hardware configurations and simulation environments. Due to the absence of standardized benchmarking parameters in the literature (such as specific motor constants and panel structural dynamics), a

Table 5. Performance summary of PID tuning using meta-heuristic algorithms.

Algorithm	Best PID [K_p, K_i, K_d]	Average cost	STD (cost)	Overshoot (mean $\pm$ std) (%)	T_s (s)	T_r (s)
GWO	[1.5126, 2.9981, 0.0100]	3.444990	0.013035	0.22 $\pm$ 0.22	1.87	1.07
AO	[1.5770, 3.0588, 0.0369]	3.446048	0.054387	0.27 $\pm$ 0.34	1.82	1.05
MRFO	[1.5691, 3.0526, 0.0266]	3.444553	0.052445	0.20 $\pm$ 0.22	1.82	1.05
HHO	[1.5270, 3.0233, 0.0100]	3.444680	0.077896	0.28 $\pm$ 0.39	1.83	1.07
GBO	[1.4094, 2.9112, 0.0100]	3.466455	0.065305	0.74 $\pm$ 1.05	1.93	1.13

Table 6. Computational and effort metrics.

Algorithm	Avg time (s)	Avg iterations	STD of iterations	Overshoot percentage	Control energy (best)
ZN-PID	-	-	-	3.8	30.8022
GWO	1.504	13.9	1.9	0.06	30.577211
AO	1.241	12.0	1.7	0.18	30.733327
MRFO	1.307	12.8	3.0	0.04	30.721350
HHO	1.283	12.6	1.6	0.06	30.645316
GBO	1.407	13.8	3.9	0.76	30.323839

Table 7. Comparison with related works.

Study	Method	OS (%)	T_s (s)	Energy	Val.
This work	GWO	0.06	< 1.90	30.3–30.7	50 runs
Mazumdar et al.[51]	GWO	0.25	> 1.2	–	None
Chauhan et al.[52]	ANN + PID	0.2	1.0	–	No
Taha et al.[11]	PSO-PID	~ 0.19	0.75	Mod.	30 runs
Rawat et al.[53]	TLBO	> 0.01	> 0.05	–	None

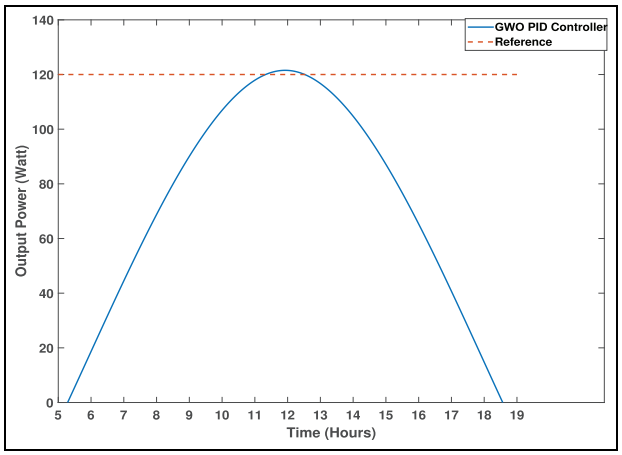

Figure 16. DASTS output power using GWO-PID controller for the daylight hours.

strictly identical re-implementation is impractical. Thus, this comparison serves primarily to position the proposed energy-aware framework qualitatively against existing methods, highlighting its competitive results.

Key findings and practical implications

The measured control energy of 30.328 V^2s represents the electrical input needed by DC motors for daily solar tracking. Given standard motor resistance values of 3–5 Ω, this equates to an actual energy use of about 30.3238—30.7332 J for each tracking adjustment. Over the long term, using smoother control methods can help minimize motor overheating, reduce wear and tear on gears and bearings, and potentially extend actuator life by 10%–15% compared to traditional single objective tuning approaches that often cause excessive oscillations. From the perspective of the PV system, cutting down on unnecessary actuator energy use increases the net energy output. In small–scale systems with 100–200 W panels, the gains are relatively small, but for larger solar farms with many dual-axis trackers, the daily savings in auxiliary energy can add up to several kilowatt-hours. This leads to a 1%–2% improvement in overall system efficiency. These findings show that the GWO-PID framework delivers real, practical advantages beyond simulation, making it valuable for real-world applications.

Conclusions

This work proposed an energy-aware, statistically validated framework for PID tuning in DASTS using five modern meta-heuristic algorithms. The tuning objective minimized both the ITAE and the control energy to ensure a balance between performance and efficiency. Simulation results from 50 Monte Carlo runs confirmed that GWO and AO deliver superior convergence speed, tracking accuracy, and energy savings compared to MRFO, HHO, and GBO. Also, the proposed framework demonstrated that the GWO as well as GBO tuned PID controllers yield the best energy efficiency–dynamic accuracy trade-off. GWO achieved the lowest overshoot (0.06%) together with the highest statistical stability (0.013 standard deviation) as well as the GBO achieved minimum control energy (30.3238 V^2s), while AO achieved the fastest convergence speed (1.241 s average runtime). Two significant features are achieved by the proposed approach: (i) It enhances both the transient and the steady state performance for precise solar alignment; and (ii) It reduces actuators effort, which extends mechanical lifespan and maximizes the energy efficiency of the tracking mechanism.

On the other hand, and despite these promising results, a key limitation of this study lies in its exclusive reliance on high-fidelity simulations without real-time or hardware-in-the-loop (HIL) implementation. While the optimization framework is designed with bounded PID parameters suitable for microcontroller deployment, practical realization poses several challenges. These include computational overhead of metaheuristics on embedded platforms, real-time constraints imposed by sampling frequency and actuator latency, signal noise robustness, and environmental uncertainties such as wind gusts or sensor drift. As a result, the main future directions will focus on hardware integration using real-time embedded controllers and closed-loop validation under realistic outdoor conditions. Additional extensions will explore adaptive or gain-scheduled PID architectures, hybrid control schemes, and multi-objective optimization with hardware-in-the-loop to validate energy-efficiency and tracking precision in practical solar energy installations.

Acknowledgement

n/a.

ORCID iD

Mohamed A. Kamel https://orcid.org/0000-0003-1968-4345

Funding

The authors received no financial support for the research, authorship, and/or publication of this article.

Declaration of conflicting interests

The authors declared no potential conflicts of interest with respect to the research, authorship, and/or publication of this article.

References

1. Sadeghi R, Parenti M, Memme S, et al. A review and comparative analysis of solar tracking systems. *Energies* 2025; 18(10): 2553. https://doi.org/10.3390/en18102553
2. (IRENA) IREA. Renewable power generation costs in 2023, https://www.irena.org/Publications/2024/Sep/Renewable-Power-Generation-Costs-in-2023 (2024, accessed 12 March 2026).
3. Zaghba L, Borni A, Benbitour MK, et al. Enhancing grid-connected photovoltaic system performance with novel hybrid MPPT technique in variable atmospheric conditions. *Sci Rep* 2024; 14(1): 8205. https://doi.org/10.1038/s41598-024-59024-4
4. Ibrahim AW, Hussein Farh HM, Fang Z, et al. A comprehensive comparison of advanced metaheuristic photovoltaic maximum power tracking algorithms during dynamic and static environmental conditions. *Heliyon* 2024; 10(18): 1–24. https://doi.org/10.1016/j.heliyon.2024.e37458
5. Ya'u Muhammad J, Tajudeen Jimoh M, Baba Kyari I, et al. A review on solar tracking system: A technique of solar power output enhancement. *Eng Sci* 2019; 4(1): 1–11. https://doi.org/10.11648/j.es.20190401.11
6. Thungsuk N, Tanaram T, Chaithanakulwat A, et al. Performance analysis of solar tracking systems by five-position angles with a single axis and dual axis. *Energies* 2023; 16(16): 1–20. https://doi.org/10.3390/en16165869
7. Bin Ishak MH, Burham N, Masrie M, et al. Automatic dual-axis solar tracking system for enhancing the performance of a solar photovoltaic panel. In: *IEEE international conference on smart instrumentation, measurement and applications (ICSIMA)*, 2023, pp. 279–283. IEEE. https://doi.org/10.1109/icsima59853.2023.10373430
8. Chapaneri K, Aly SP, John JJ, et al. Tracking the sun: performance analysis of single-axis vs dual-axis solar PV systems in uae desert climate. In: *Middle East and North Africa Solar Conference (MENA-SC)*, 2023, pp. 1–3. IEEE. https://doi.org/10.1109/mena-sc54044.2023.10374532
9. Issa HA, Abdali LM, Alhusseini H, et al. Design, modeling, and control of a dual-axis solar tracker using fractional order PID controllers for enhanced energy efficiency. *Results in Engineering* 2025; 27: 106073. https://doi.org/10.1016/j.rineng.2025.106073
10. Hai T, Zhou J and Furukawa N. Performance enhancement of fuzzy-pid controller for MPPT of PV system to extract maximum power under different conditions. *Soft Comput* 2024; 28(3): 2035–2054. https://doi.org/10.1007/s00500-023-09171-z
11. Taha MI, Kamel MA, Said E, et al. Performance analysis of dual-axis solar tracking system using fuzzy logic and optimized PID control strategies. In: *International conference on electrical engineering (ICEENG)*, 2025, pp. 1–6. IEEE. https://doi.org/10.1109/iceeng64546.2025.11031283
12. AL-Rousan N, Mat Isa NA and Mat Desa MK. Efficient single and dual axis solar tracking system controllers based on adaptive neural fuzzy inference system. *J King Saud Univ - Eng Sci* 2020; 32(7): 459–469. https://doi.org/10.1016/j.jksues.2020.04.004
13. Werku C. *Design of optimal fuzzy-PID controller for dual axis sun tracking system*. Master's Thesis, Addis Ababa Science and Technology University, 2021.
14. Moyo RT and Dewa M. The role of computational intelligence techniques in the advancements of solar photovoltaic systems for sustainable development: a review. *Renew Energy Sustain Dev* 2022; 8(2): 52–69. https://doi.org/10.21622/resd.2022.08.2.052
15. Joseph SB, Dada EG, Abidemi A, et al. Metaheuristic algorithms for PID controller parameters tuning: review, approaches and open problems. *Heliyon* 2022; 8(5): e09399. https://doi.org/10.1016/j.heliyon.2022.e09399
16. Nassef AM, Abdelkareem MA, Maghrabie HM, et al. Metaheuristic-based algorithms for optimizing fractional-order controllers—a recent, systematic, and comprehensive review. *Fractal Fract* 2023; 7(7): 1–30. https://doi.org/10.3390/fractalfract7070553
17. Mostafa RR, Houssein EH, Hussien AG, et al. An enhanced chameleon swarm algorithm for global

optimization and multi-level thresholding medical image segmentation. *Neural Comput Appl* 2024; 36(15): 8775–8823. https://doi.org/10.1007/s00521-024-09524-1
18. Singh M, Arora S and Shah OA. Enhancing hybrid power system performance with gwo-tuned fuzzy-pid controllers: a comparative study. *Int J Robot Control Syst* 2024; 4(2): 709–726. https://doi.org/10.31763/ijrcs.v4i2.1388
19. Taleb SM, Yasin ET, Saadi AA, et al. A comprehensive survey of aquila optimizer: theory, variants, hybridization, and applications. *Arch Comput Methods Eng* 2025; 32: 4643–4689. https://doi.org/10.1007/s11831-025-10281-0
20. Güven AF and Mengi OÖ. Nature-ınspired algorithms for optimizing fractional order PID controllers in time-delayed systems. *Optim Control Appl Methods* 2024; 45(3): 1251–1279. https://doi.org/10.1002/oca.3101
21. Hassan IH, Abdullahi M, Isuwa J, et al. A comprehensive survey of honey badger optimization algorithm and meta-analysis of its variants and applications. *Franklin Open* 2024; 8: 1–30. https://doi.org/10.1016/j.fraope.2024.100141
22. Abdullahi M, Hassan IH, Abdullahi MD, et al. Manta ray foraging optimization algorithm: modifications and applications. *IEEE Access* 2023; 11: 53315–53343. https://doi.org/10.1109/access.2023.3276264
23. Güven AF, Mengi OÖ, Elseify MA, et al. Comprehensive optimization of pid controller parameters for dc motor speed management using a modified jellyfish search algorithm. *Optim Control Appl Methods* 2024; 46(1): 320–342. https://doi.org/10.1002/oca.3218
24. Alexandru C. Simulation and optimization of a dual-axis solar tracking mechanism. *Mathematics* 2024; 12(7): 1–32. https://doi.org/10.3390/math12071034
25. Menaka D, PPN, An effective energy production and analysis in a solar tracking system. *J Electr Syst* 2024; 20(3s): 2127–2139. https://doi.org/10.52783/jes.1812
26. Widyaningrum VT, Romadhon AS and Safitri D. Solar tracking system dual axis using proportional integral derivative (pid) controller. In: *IEEE information technology international seminar (ITIS)*, 2023, pp. 1–5. IEEE. https://doi.org/10.1109/itis59651.2023.10420258
27. Cikan M and Dogansahin K. A comprehensive evaluation of up-to-date optimization algorithms on MPPT application for photovoltaic systems. *Energy Sour Part A: Recov Utilization Environ Effects* 2023; 45(4): 10381–10407. https://doi.org/10.1080/15567036.2023.2245771
28. S M and Jebaseelan S. A comprehensive comparative study on intelligence based optimization algorithms used for maximum power tracking in grid-PV systems. *Sustain Comput Inform Syst* 2024; 41: 100946. https://doi.org/10.1016/j.suscom.2023.100946
29. Alhusseini H, Abdali LM, Issa HA, et al. Adaptive particle swarm optimization based model predictive control MPPT algorithm for pv systems under partial shading conditions. *Results Eng* 2025; 28: 107419. https://doi.org/10.1016/j.rineng.2025.107419
30. Güven AF. Exploring solar energy systems: a comparative study of optimization algorithms, MPPTs, and controllers. *IET Control Theory Appl* 2024; 18(7): 887–920. https://doi.org/10.1049/cth2.12626
31. Yasser H, Abdellatif S, Yacine B, et al. An integrated multi-objective optimization algorithm for parameter estimation and maximum power point tracking in photovoltaic systems. In: *International conference on advanced electrical engineering (ICAEE)*, 2024, pp. 1–6. IEEE. https://doi.org/10.1109/icaee61760.2024.10783216
32. Madhusudhan P, Mishra P, Vanya Sree G, et al. *Metaheuristic optimization for enhancing the thermal performance of solar energy devices*. Chapter 6. IGI Global, 2024, pp. 107–128. https://doi.org/10.4018/979-8-3693-3314-3.ch006.
33. Ontiveros JJ, Ávalos CD, Loza F, et al. Evaluation and design of power controller of two-axis solar tracking by PID and FL for a photovoltaic module. *Int J Photoenergy* 2020; 2020: 1–13. https://doi.org/10.1155/2020/8813732
34. Reda I and Andreas A. Solar position algorithm for solar radiation applications. Technical Report NREL/TP-560-34302, National Renewable Energy Laboratory (NREL), 2008.
35. El Hammoumi A, Chtita S, Motahhir S, et al. Solar PV energy: from material to use, and the most commonly used techniques to maximize the power output of PV systems: A focus on solar trackers and floating solar panels. *Energy Rep* 2022; 8: 11992–12010. https://doi.org/10.1016/j.egyr.2022.09.054
36. Gilman P. Sam photovoltaic model technical reference. Technical Report NREL/TP-6A20-64102, National Renewable Energy Laboratory, 2015.
37. Hassanian R, Riedel M, Yeganeh N, et al. A practical approach for estimating the optimum tilt angle of a photovoltaic panel for a long period—experimental recorded data. *Sola* 2021; 1(1): 41–51. https://doi.org/10.3390/solar1010005
38. Chandramouli A and Sivachidambaranathan RV. Modelling and design of five parameter single diode photovoltaic model with artificial intelligent MPPT power system. *Int J Recent Technol Eng* 2019; 8(2S8): 1063–1068. https://doi.org/10.35940/ijrte.b1014.0882s819
39. Reddy VSS, Kruthika U and Paneerselvam S. Optimal PID tuning for solar tracking system using bio-inspired algorithms. In: *International conference on trends in sustainable computing and machine intelligence*, 2024, pp. 25–42. https://doi.org/10.1007/978-981-96-1452-3_3
40. Singh K and Saini MK. An insight into recent advances in the intelligent controller methods. In: *International conference on data science and applications*. Springer Nature, 2023, pp. 85–95. https://doi.org/10.1007/978-981-99-7817-5_7
41. Maghfiroh H, Ataka A, Wahyunggoro O, et al. Optimal energy control of dc motor speed control: comparative study. In: *International conference on computer, control, informatics and its applications (IC3INA)*, 2013, pp. 89–93. IEEE. https://doi.org/10.1109/ic3ina.2013.6819154
42. Hu H, Xu L, Wei R, et al. Multi-objective control optimization for greenhouse environment using evolutionary algorithms. *Sensors* 2011; 11(6): 5792–5807. https://doi.org/10.3390/s110605792
43. Mirjalili S, Mirjalili SM and Lewis A. Grey wolf optimizer. *Adv Eng Softw* 2014; 69: 46–61. https://doi.org/10.1016/j.advengsoft.2013.12.007
44. Abualigah L, Yousri D, Abd Elaziz M, et al. Aquila optimizer: a novel meta-heuristic optimization algorithm. *Comput Ind Eng* 2021; 157: 107250. https://doi.org/10.1016/j.cie.2021.107250
45. Ren L, Wang D and Zhang Y. Optimal control of FSBB converter with aquila optimizer-based PID controller.

Micromachines 2024; 15(10): 1277. https://doi.org/10.3390/mi15101277
46. Zhao W, Zhang Z and Wang L. Manta ray foraging optimization: an effective bio-inspired optimizer for engineering applications. *Eng Appl Artif Intell* 2020; 87: 103300. https://doi.org/10.1016/j.engappai.2019.103300
47. Heidari AA, Mirjalili S, Faris H, et al. Harris hawks optimization: algorithm and applications. *Future Gener Comput Syst* 2019; 97: 849–872. https://doi.org/10.1016/j.future.2019.02.028
48. Roy R, Mukherjee V and Singh RP. Harris hawks optimization algorithm for model order reduction of interconnected wind turbines. *ISA Trans* 2022; 128: 372–385. https://doi.org/10.1016/j.isatra.2021.09.019
49. Daoud MS, Shehab M, Al-Mimi HM, et al. Gradient-based optimizer (gbo): a review, theory, variants, and applications. *Arch Comput Methods Eng* 2023; 30(4): 2431–2449. https://doi.org/10.1007/s11831-022-09872-y
50. Terán-García E and Pérez-Fernández R. A robust alternative to the lilliefors test of normality. *J Stat Comput Simul* 2024; 94(7): 1494–1512. https://doi.org/10.1080/00949655.2023.2291138
51. Mazumdar D, Shuaibu HA, Sain C, et al. A novel and sturdy MPPT architecture for grid-tied EV charging stations using ali baba and forty thieves optimization. *Discov Sustain* 2025; 6(1): 159–171. https://doi.org/10.1007/s43621-025-01089-w
52. Chauhan AS, Joshi DK and Sharma NK. Design of a novel optimal control energy management strategy for stand alone hybrid solar-wind system. *Int J Tech Res Sci* 2024; 9(06): 1–14. https://doi.org/10.30780/ijtrs.v09.i06.001
53. Rawat A, Jha SK and Kumar B. Position controlling of sun tracking system using optimization technique. *Energy Rep* 2020; 6: 304–309. https://doi.org/10.1016/j.egyr.2019.11.079